ACS APPLIED MATERIALS & INTERFACES

Research Article

www.acsami.org

Probing the Interfacial Interaction in Layered-Carbon-Stabilized Iron Oxide Nanostructures: A Soft X-ray Spectroscopic Study

Hui Zhang,[†,‡] Jinyin Liu,[†] Guanqi Zhao,[†] Yongjun Gao,[§] Tolek Tyliszczak,[‡] Per-Anders Glans,[‡] Jinghua Guo,*[,‡] Ding Ma,*[,§] Xu-Hui Sun,[†] and Jun Zhong*[,†]

[†]Soochow University-Western University Centre for Synchrotron Radiation Research, Institute of Functional Nano and Soft Material (FUNSOM) and Collaborative Innovation Center of Suzhou Nano Science & Technology, Soochow University, Suzhou 215123, China

[‡]Advanced Light Source, Lawrence Berkeley National Laboratory, Berkeley, California 94720, United States

[§]Beijing National Laboratory for Molecular Sciences, College of Chemistry and Molecular Engineering, Peking University, Beijing 100871, China

Supporting Information

ABSTRACT: We have stabilized the iron oxide nanoparticles (NPs) of various sizes on layered carbon materials (Fe-oxide/C) that show excellent catalytic performance. From the characterization of X-ray absorption spectroscopy (XAS), X-ray emission spectroscopy (XES), scanning transmission X-ray microscopy (STXM) and X-ray magnetic circular dichroism spectroscopy (XMCD), a strong interfacial interaction in the Fe-oxide/C hybrids has been observed between the small iron oxide NPs and layered carbon in contrast to the weak interaction in the large iron oxide NPs. The interfacial interaction between the NPs and layered carbon is found to link with the improved catalytic performance. In addition, the Fe *L*-edge XMCD spectra show that the large iron oxide NPs are mainly γ-Fe_2O_3 with a strong ferromagnetic property, whereas the small iron oxide NPs with strong interfacial interaction are mainly α-Fe_2O_3 or amorphous Fe_2O_3 with a nonmagnetic property. The results strongly suggest that the interfacial interaction plays a key role for the catalytic performance, and the experimental findings may provide guidance toward rational design of high-performance catalysts.

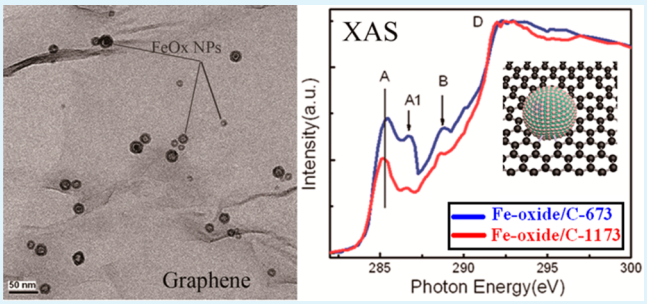

KEYWORDS: *interfacial interaction, soft X-ray spectroscopy, iron oxide, layered carbon, catalysts, magnetic property*

1. INTRODUCTION

Layered carbon materials based on one or a few graphene layers have been widely reported for applications of catalysis, energy conversion and energy storage owing to their unique structure.[1−5] Recently, layered carbon materials were reported to be good supporting materials for the nanoparticles (NPs) in energy-related applications.[6−11] For example, the hybrids of nanostructured $LiMn_xFe_{1-x}PO_4$ and graphene as a cathode material significantly enhanced the performance of the Li-ion battery.[7,8,10] The combination of Co_3O_4 nanocrystals and N-doped graphene oxide also showed unexpected high oxygen reduction reaction (ORR) activity.[6] Although many hybrid materials with high efficiency have been investigated,[6,10−12] the key question of why the combination of layered carbon and the NPs exhibits such an unique enhancement of the performance still remains to be answered. Due to the complexity of carbon-based materials such as the existence of amorphous carbon, defects sites, surface modification or contaminations, catalyst residues or the aggregated NPs, the effective factors responsible for the improved performance are still under debate.

Here we investigate the electronic structure of the layered-carbon-stabilized iron oxide nanostructures (Fe-oxide/C) to understand the enhanced performance in these hybrids. The Fe-oxide/C hybrids presented high catalytic activity in the oxidation reactions.[9] By tuning the annealing temperature, the NP size and structure in the hybrids could be readily selected. The catalytic performance of the selectivity and conversion rate was strongly size-dependent in catalyzing the oxidation of cyclohexanol.[9] Thus, it is a good choice of the modeling system to evaluate how the electronic structure affects the catalytic performance.

Soft X-ray spectroscopic methods such as X-ray absorption spectroscopy (XAS), X-ray emission spectroscopy (XES), scanning transmission X-ray microscopy (STXM) and X-ray magnetic circular dichroism spectroscopy (XMCD) were used to systematically investigate the electronic structure of Fe-oxide/C hybrids. X-ray spectroscopies are element-specific

Received: October 25, 2014
Accepted: April 3, 2015
Published: April 3, 2015

DOI: 10.1021/am5073996
ACS Appl. Mater. Interfaces 2015, 7, 7863−7868

techniques, which are unique to characterize the complex systems.[13] XAS probes the unoccupied density of states (DOS) whereas XES probes the occupied DOS.[13,14] Both XAS and XES have been frequently used for the electronic structure study of nanomaterials.[13] STXM provides the chemical information through the XAS and microscopic imaging with a spatial resolution of typically 25 nm.[12,15−17] XMCD reveals the spin dependence in the XAS spectra, which offers abundant magnetic information.[18]

By combining all these soft X-ray spectroscopic techniques, a good description of the electronic structure of the Fe-oxide/C hybrids can be obtained. Especially, a strong interfacial interaction was observed between the small iron oxide NPs and layered carbon in contrast to the weak interaction in the large iron oxide NPs. The strong interfacial interaction led to better catalytic performance. XMCD results also showed that the large NPs were mainly γ-Fe_2O_3 with a strong ferromagnetic property, whereas the small NPs with strong interfacial interaction were mainly α-Fe_2O_3 with a nonmagnetic property.

2. EXPERIMENTAL SECTION

2.1. Materials Preparation. The layered-carbon-stabilized iron oxide nanostructures, called Fe-oxide/C hybridized materials, were synthesized from the self-assembled ferrocene and the oxide form of layered carbon, followed by annealing to high temperatures.[9] A detailed description of the synthesis process was published in ref 9. In brief, the graphene oxide (GO) was prepared by a modified Hummer's method, and the GO−ferrocenium powder was obtained from the self-assembled ferrocene and the GO in the nitric acid solution. The GO−ferrocenium powder was then quickly heated to a designed temperature (T_d) under H_2 flow for 1 min. When T_d was higher than 673 K, the iron oxide NPs was obtained on layered carbon (labeled as Fe-oxide/C-673), and a series of samples with different T_d values (labeled as Fe-oxide/C-673, Fe-oxide/C-773, Fe-oxide/C-973 and Fe-oxide/C-1173) were prepared.

2.2. Characterization. C *K*-edge XAS and XES measurements were performed on BL8.0.1 (wet-RIXS endstation) of the Advanced Light Source (ALS), Lawrence Berkeley National Laboratory.[13] The spot size is set to about 0.5 × 0.5 mm. The energy resolution is 0.2 eV for C *K*-edge XAS and it is 0.3 eV for XES measurements. For XAS measurements, the incident angle is about 45° to the sample surface. The XES spectrometer is orthogonal to incoming photon beam. The C *K*-edge XAS analysis was recorded in total-electron-yield (TEY) mode and energy calibration was by aligning the π^* peak at 285.5 eV for the reference samples: highly oriented pyrolitic graphite. The C *K*-edge XES analysis recorded by using a Nordgren-type spectrometer.[19] Fe *L*-edge XAS and XMCD experiments were performed on BL6.3.1 of the ALS. The XMCD is the difference signal between the XAS spectra with circular polarization of the X-rays parallel ($\sigma\uparrow$) and antiparallel ($\sigma\downarrow$) to the applied magnetic field, $\sigma_{XMCD} = \sigma\downarrow - \sigma\uparrow$.[18] XMCD spectra were measured at room temperature and 2T magnetic fields parallel to incoming X-ray beam. The Fe-oxide/C powders were pressed on a Cu tape for XAS and XMCD experiments.

The Fe-oxide/C powders were sonically dispersed on the TEM grid (Cu grid with lacey carbon) for STXM experiments.[15] The STXM experiments were performed on the SM beamline of the Canaidan Light Source (CLS). A circularly polarized X-ray beam perpendicular to the sample surface was used. The focused X-ray beam was about 25 nm and the photon flux was about 2×10^7 photons/s. The data were analyzed by aXis2000 software (http://unicorn.mcmaster.ca/aXis2000.html).[16]

3. RESULTS AND DISCUSSION

Figure 1 shows the TEM images of Fe-oxide/C samples treated at 673, 773 and 1173 K, respectively. The morphology of Fe-oxide/C samples shows a strong dependence on the annealing

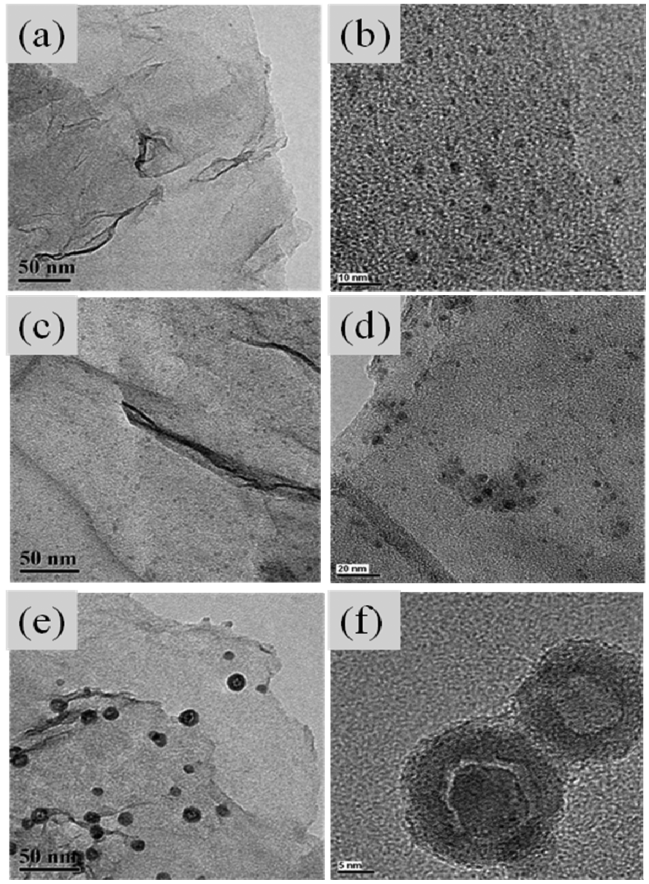

Figure 1. TEM images of Fe-oxide/C samples synthesized at different temperatures. (a and b) Fe-oxide/C-673; (c and d) Fe-oxide/C-773; (e and f) Fe-oxide/C-1173. The scale bars in panels a, c and e are all 50 nm. The scale bars in panels b, d and f are 10, 20 and 5 nm, respectively.

temperature T_d. At the lower temperature such as 673 K, the formed iron oxide NPs are very small. The average size of the NPs is around 2 nm in Fe-oxide/C-673 with a narrow size distribution. The average size of the NPs in Fe-oxide/C-673 is also around 2 nm, but some large NPs (about 5 nm) can also be observed. When the temperature increases, the size of NPs also increases significantly. Especially, when the temperature reaches 1173 K, the NPs grow to be about 20 nm. The large NPs treated at 1173 K also show different morphology such as core-void-shell and hollow structures (Figure 1f) due to the Kirkendall effect.[9] The average size of the hollow NPs is around 10 nm whereas the core-void-shell NPs have a size distribution of around 14−25 nm. More details about the NPs can be found in ref 9. We have not shown the samples treated at below 673 K because there was no significant NPs observed in those samples.[9]

The C *K*-edge XAS spectra of Fe-oxide/C samples treated at 673, 773, 973 and 1173 K are shown in Figure 2a (the spectra have been normalized to the pre-edge and the postedge at about 310 eV). The XAS spectra with a long energy scale are also shown in Figure 2c. All the spectra of Fe-oxide/C samples show similar spectral profile with three main absorption peaks labeled as A, B and D in Figure 2a. The three peaks have been widely studied in carbon materials.[19−22] Peak A at about 285.5 eV can be assigned to the π^* (C═C) feature from aromatic ring structure of layered carbon whereas peak D at about 291.7

DOI: 10.1021/am5073996
ACS Appl. Mater. Interfaces 2015, 7, 7863−7868

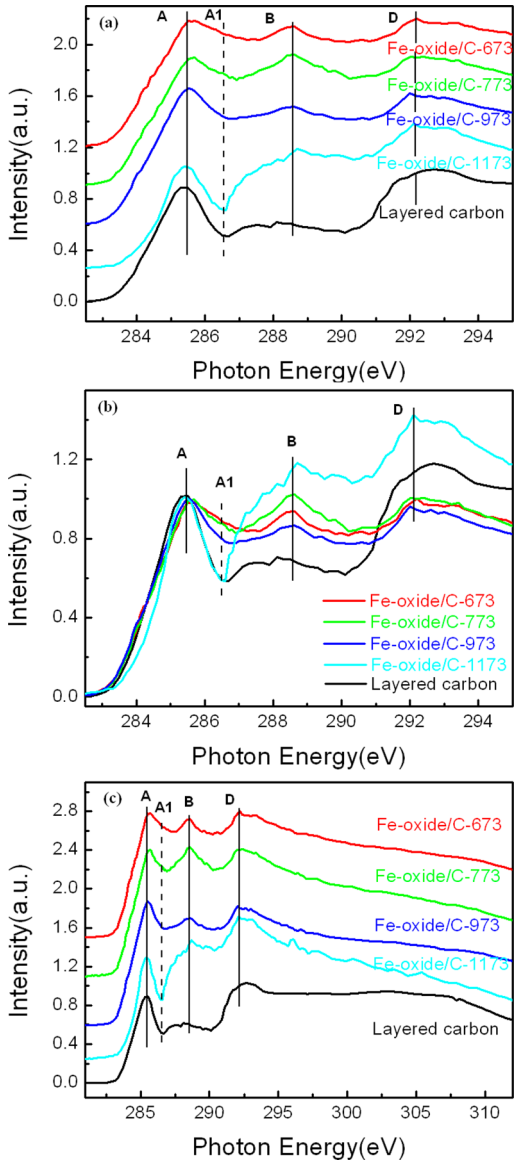

Figure 2. (a) C *K*-edge XAS spectra of layered carbon, Fe-oxide/C-673, Fe-oxide/C-773, Fe-oxide/C-973 and Fe-oxide/C-1173 (normalized at around 310 eV). The dash line shows the evolution of feature A1 at various annealing temperatures. (b) Magnified C *K*-edge XAS spectra of layered carbon, Fe-oxide/C-673, Fe-oxide/C-773, Fe-oxide/C-973 and Fe-oxide/C-1173 (normalized at the feature A around 285.5 eV). (c) C *K*-edge XAS spectra of layered carbon, Fe-oxide/C-673, Fe-oxide/C-773, Fe-oxide/C-973 and Fe-oxide/C-1173 with a long energy scale.

eV can be assigned to the σ^* feature of layered carbon.[21,22] Peak B at about 288 eV is attributed to the oxidized groups such as C═O or COOH.[21,22] The XAS spectra suggest that the Fe-oxide/C hybrids have aromatic carbon ring structure and have been heavily oxidized during the synthesis process or after thermal treatment when exposed to air. Although all samples show the similar spectral shape, one subtle difference can be seen as guided by the dotted line: a reduced absorption intensity as indicated by A1 when annealing temperature increases to 1173 K. We also show the magnified spectra in Figure 2b to reveal the evolution of feature A1 (normalized at the feature A). In previous reports, the feature A1 in C *K*-edge XAS spectrum was reported and attributed to the interaction between the NPs and carbon nanotubes (Sn—O—C bonds).[23] Fe-catalyzed carbon nanotubes also showed a similar XAS feature, indicating a strong hybridization between C and Fe.[24] Nanomaterials may have great potential to interact with the surrounding materials. For example, recently the nanodiamonds dispersed in water were reported to show interfacial charge transfer to the surrounding water molecules, which resulted in valence holes in the nanodiamonds.[25] In this study, the evolution of feature A1 with the temperature points to the interfacial interaction between the iron oxide NPs and layered carbon. When the annealing temperature is low, the NPs are very small and they are chemically active to form the chemical bonds such as Fe—O—C. The energy position of the feature A1 shifts slightly from the π^* feature, indicating the chemical interaction is not very strong. When the annealing temperature increases, the iron oxide NPs grow and aggregate to be large particles of lower chemical activity (similar to bulk materials), thus the interaction between the NPs and layered carbon is further reduced. The evolution of feature A1 in Figure 2 shows the strong chemical dependence on the annealing temperature, which provides the evidence of interfacial interaction between the small iron oxide NPs and layered carbon.

To identify clearly the interfacial interaction between the iron oxide NPs and layered carbon, STXM experiments are performed in accordance to the TEM images. TEM reveals the detailed structure with high spatial resolution. The combination of STXM and TEM probes the NPs and layered carbon in the detected region and distinguishes the contribution of impurities such as amorphous carbon or the aggregation of NPs.[17] In Figure 3, we show side-by-side the TEM and STXM images of Fe-oxide/C-673 and Fe-oxide/C-1173. Figure 3a,b shows the TEM image and the corresponding STXM map of Fe-oxide/C-673, whereas Figure 3d,e shows the TEM image and the corresponding STXM map of Fe-oxide/C-1173. Figure 3c,f shows the magnified TEM images of Fe-oxide/C-673 and Fe-oxide/C-1173 marked by gray ellipse in Figure 3a,d to confirm the composition in the corresponding detected region. It is clear that the detected region consists of the NPs and layered carbon with no obvious impurities such as amorphous carbon or the aggregation of NPs. Figure 3g shows the STXM C *K*-edge XAS spectra of Fe-oxide/C-673 and Fe-oxide/C-1173 obtained from the marked areas in Figure 3b,d, respectively. The STXM XAS spectra of both samples show a similar spectral shape with three main features A, B and D, as shown in Figure 2. There are some differences in the XAS spectral shapes between Figure 2 and Figure 3 such as the different intensity ratios of feature A and feature D. Because in STXM experiments, the incident X-ray is perpendicular to the sample surface whereas in the classic XAS experiments, the X-ray has an incident angle of about 45° to the sample surface, the different incident angles might be responsible for the different spectral shapes between Figure 2 and Figure 3.[22] The spectrum of Fe-oxide/C-673 in Figure 3g shows a prominent feature A1, indicating the existence of interfacial interaction between the NPs and layered carbon. The feature A1 in the spectrum of Fe-oxide/C-1173 also decreases sharply indicating the weak interaction for the large NPs.

The interfacial interaction could be related to the excellent catalytic performance. Actually, although all the Fe-oxide/C hybrids show good selectivity and conversion rate in catalyzing the oxidation of secondary alcohols, Fe-oxide/C-673 has the highest activity.[9] Our results show that Fe-oxide/C-673 is also the sample with the strongest interfacial interaction, thus the

DOI: 10.1021/am5073996
ACS Appl. Mater. Interfaces 2015, 7, 7863−7868

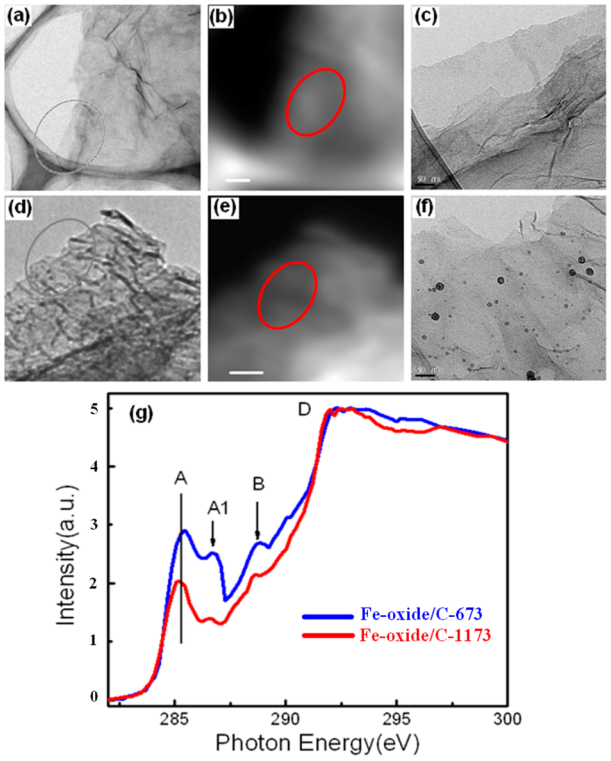

Figure 3. (a and b) TEM image and the corresponding STXM image of Fe-oxide/C-673, respectively. (c) Magnified TEM image marked as a gray ellipse in panel a. (d and e) TEM image and the corresponding STXM image of Fe-oxide/C-1173, respectively. (f) Magnified TEM image marked as a gray ellipse in panel d. (g) STXM C *K*-edge XAS spectra of Fe-oxide/C-673 and Fe-oxide/C-1173 from the corresponding regions in panels b and e labeled as red circles. The scale bar in panels b and e is 200 nm.

synergetic effects between the NPs and C in Fe-oxide/C-673 can be expected to be related to the excellent catalytic performance.

XES measurements are also performed to obtain the information on occupied DOS of Fe-oxide/C hybrids. Nonresonant XES spectra of Fe-oxide/C-673 and Fe-oxide/C-1173 are shown in Figure 4. The nonresonantly excited XES spectra are collected with an excitation energy of 305 eV and the spectra of both samples show a wide emission band centered at 276 eV and a high-energy peak centered at 281 eV, which result from σ and π states, respectively.[13,14] The nonresonantly excited spectra of Fe-oxide/C-673 and Fe-oxide/C-1173 are nearly identical to each other, indicating that no obvious band structure change between the two samples under the present energy resolution. The resonant XES spectra are also recorded and shown in the Supporting Information, Figure S1.[13,14,26,27] The resonant XES spectra of Fe-oxide/C-673 and Fe-oxide/C-1173 are very similar to each other, except for the small difference around 282 eV in the XES spectra with an excitation energy of 285.5 eV. According to the reference, the control over excitation energy allows one to select the crystal momentum of the photoelectron's final state in the conduction band.[26] Since the excitation energy of 285.5 eV is just above Fermi level, the observed difference in the XES spectra can be attributed to the slightly different band structure near *K* point between the two samples.[26]

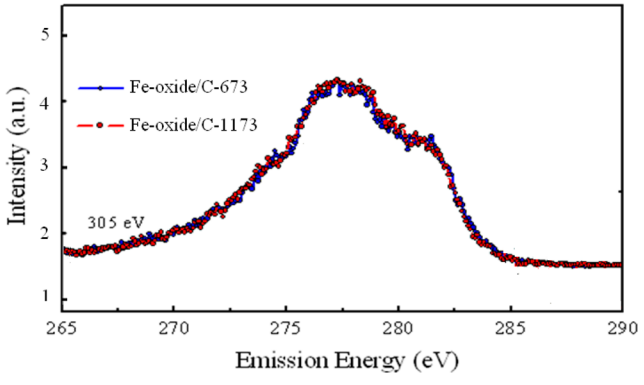

Figure 4. XES spectra of Fe-oxide/C-673 and Fe-oxide/C-1173 excited at 305 eV.

The magnetic properties of Fe-oxide/C hybrids are also investigated by XMCD. Figure 5a,b displays the Fe $L_{2,3}$-edge XAS and XMCD spectra, respectively. The Fe *L*-edge XAS spectra show two regions due to the orbital splitting. The XAS spectral shapes for all Fe-oxide/C hybrids are very similar. In the L_3 region, the main peak is at around 709 eV (labeled as A′) with a shoulder peak at around 708 eV (labeled as A). The spectral shape is similar to that for Fe_2O_3 or Fe_3O_4.[18,28] Here the energy resolution is not very high due to the equipment or the small particle size and the integrated peak A can not be used to identify Fe_3O_4 or Fe_2O_3.

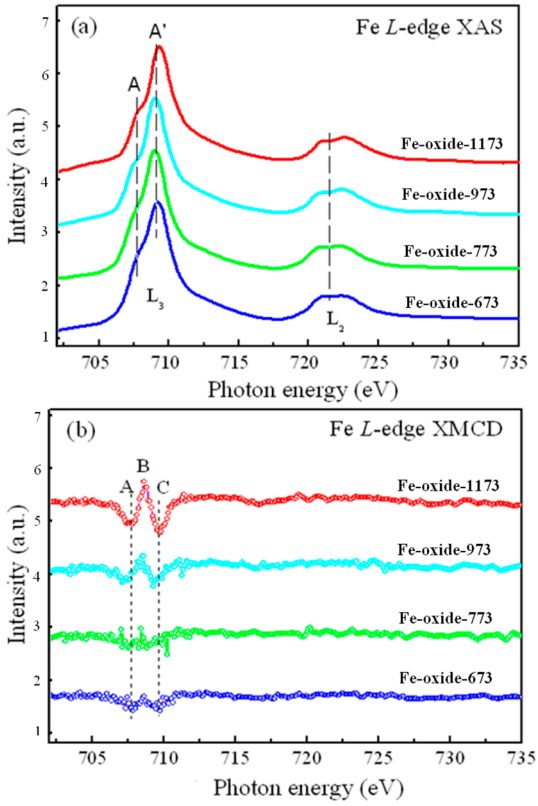

Figure 5. (a) Fe $L_{2,3}$-edge XAS and (b) the corresponding XMCD spectra of Fe-oxide/C samples synthesized at different temperatures.

The XMCD spectra in Figure 5b exhibit significant differences in spectral profile depending on the annealing temperature. XMCD has been widely used to investigate the magnetic property and applied to distinguish various ferromagnetic phases that contribute to different dichroic

DOI: 10.1021/am5073996
ACS Appl. Mater. Interfaces 2015, 7, 7863−7868

signals in iron systems.[18,28−30] The dichroic signal of Fe-oxide/C-673 is insignificant, suggesting weak magnetic property of the sample. The NPs in Fe-oxide/C-673 could be mainly α-Fe_2O_3 or amorphous Fe_2O_3 with nonmagnetic property, as Fe_3O_4 or γ-Fe_2O_3 will show strong ferromagnetic property.[18] For the sample of Fe-oxide/C-773, the dichroic signal is still weak and may suggest that the NPs have no change to the α-Fe_2O_3 or amorphous Fe_2O_3 phases. When the temperature increases to 973 K, a significant dichroic signal is observed, indicating there is a change to the crystalline phase in the sample. We used three peaks labeled as A, B and C to identify the XMCD features. According to the references, the peaks B and C can be related to the oxidation state of Fe^{3+} while the peak A is typically related to the oxidation state of Fe^{2+}.[18,31] Here peak A is lower than peak C, suggesting mainly Fe^{3+} components in the sample. Thus, the results suggest that the NPs in Fe-oxide/C-973 are mainly γ-Fe_2O_3 with both Fe^{3+} and strong ferromagnetic property. An important phase transition from α-Fe_2O_3 or amorphous Fe_2O_3 to γ-Fe_2O_3 occurs when the annealing temperature increases to 973 K or above. Looking at the A/C ratios, the Fe-oxide/C samples at lower temperatures such as 673 and 773 K have a ratio of about 1 (though the peaks are weak) whereas the samples at 973 and 1173 K have a ratio obviously less than 1, indicating that the samples at lower temperatures may have some Fe^{2+} contents. Also, the slight shift of peak A′ in Figure 5a for the Fe-oxide/C-1173 sample supports the hypothesis. The presence of some Fe^{2+} contents can be related to the interfacial interaction with charge redistribution. When the NPs grow with further increased temperature, core-void-shell structures due to the Kirkendall effect are observed from the hard X-ray XAS spectra.[9] The inside core can be Fe species with low oxidation state such as Fe_3O_4. Our results from soft X-ray spectroscopy reveal mainly the surface property and the interface structure of the NPs. For the sample treated at 1173 K with large NPs, a strong dichroic signal is observed with a similar spectral shape as that of Fe-oxide/C-973, pointing to the existence of γ-Fe_2O_3. When the annealing temperature increases, the size of the NPs in Fe-oxide/C hybrids increases and the magnetic property also becomes strong. The interfacial interaction between the NPs and layered carbon decreases with the growth of the NPs. The α-Fe_2O_3 or amorphous Fe_2O_3 phases of small NPs may favor the interfacial interaction and improve the catalytic performance.

4. SUMMARY

In summary, we have investigated the electronic structure of Fe-oxide/C hybrids by using soft X-ray techniques such as XAS, STXM, XES and XMCD. An interfacial interaction between the iron oxide NPs and layered carbon was clearly identified by XAS and STXM with a prominent feature A1 in the C *K*-edge XAS spectra. Results showed that the small NPs led to the strong interfacial interaction whereas the large NPs resulted in the weak interaction. Moreover, the strong interfacial interaction could be related to the improved catalytic performance. XMCD results at the Fe *L*-edge also revealed that the large NPs were mainly γ-Fe_2O_3 whereas the small NPs were mainly α-Fe_2O_3 or amorphous Fe_2O_3 with a nonmagnetic property.

■ ASSOCIATED CONTENT

Supporting Information

Resonant XES spectra of Fe-oxide/C-673 and Fe-oxide/C-1173. This material is available free of charge via the Internet at http://pubs.acs.org.

■ AUTHOR INFORMATION

Corresponding Authors

*J. Guo. E-mail: jguo@lbl.gov.
*D. Ma. E-mail: Dma@pku.edu.cn.
*J. Zhong. E-mail: jzhong@suda.edu.cn.

Notes

The authors declare no competing financial interest.

■ ACKNOWLEDGMENTS

We acknowledge the support from CLS and ALS. We thank J. Wang, C. Karunakaran and Y. Lu for their support of experiments at CLS. Research at CLS is supported by NSERC, NRC, CIHR, and the University of Saskatchewan. The work at ALS is supported by the U.S. Department of Energy under the Contract No. DE-AC02-05CH11231. We acknowledge the National Basic Research Development Program of China (2012CB825800, 2010CB934500), the National Natural Science Foundation of China (11275137, 11179032, 91333112) and the Priority Academic Program Development of Jiangsu Higher Education Institutions (PAPD). This is also a project supported by the Fund for Innovative Research Teams of Jiangsu Higher Education Institutions.

■ REFERENCES

(1) Geim, A. K.; Novoselov, K. S. The Rise of Graphene. *Nat. Mater.* **2007**, *6*, 183−191.
(2) Stankovich, S.; Dikin, D. A.; Piner, R. D.; Kohlhaas, K. A.; Kleinhammes, A.; Jia, Y.; Wu, Y.; Nguyen, S. T.; Ruoff, R. S. Synthesis of Graphene-based Nanosheets via Chemical Reduction of Exfoliated Graphite Oxide. *Carbon* **2007**, *45*, 1558−1565.
(3) Stankovich, S.; Dikin, D. A.; Dommett, G. H. B.; Kohlhaas, K. M.; Zimney, E. J.; Stach, E. A.; Piner, R. D.; Nguyen, S. T.; Ruoff, R. S. Graphene-based Composite Materials. *Nature* **2006**, *442*, 282−286.
(4) Gao, Y.; Hu, G.; Zhang, W.; Ma, D.; Bao, X. π-π Interaction Intercalation of Layered Carbon Materials with Metallocene. *Dalton Trans.* **2011**, *40*, 4542−4547.
(5) Gao, Y.; Hu, G.; Zhong, J.; Shi, Z.; Zhu, Y.; Su, D.; Wang, J.; Bao, X.; Ma, D. Nitrogen-Doped sp^2-Hybridized Carbon as a Superior Catalyst for Selective Oxidation. *Angew. Chem., Int. Ed.* **2013**, *52*, 2109−2113.
(6) Liang, Y.; Li, Y.; Wang, H.; Zhou, J.; Wang, J.; Regier, T.; Dai, H. Co_3O_4 Nanocrystals on Graphene as a Synergistic Catalyst for Oxygen Reduction Reaction. *Nat. Mater.* **2011**, *10*, 780−786.
(7) Wang, H. L.; Yang, Y.; Liang, Y. Y.; Cui, L. F.; Casalongue, H. S.; Li, Y. G.; Hong, G. S.; Cui, Y.; Dai, H. J. $LiMn_{1-x}Fe_xPO_4$ Nanorods Grown on Graphene Sheets for Ultrahigh-Rate-Performance Lithium Ion Batteries. *Angew. Chem., Int. Ed.* **2011**, *50*, 7364−7368.
(8) Yang, J. J.; Wang, J. J.; Tang, Y. J.; Wang, D. N.; Li, X. F.; Hu, Y. H.; Li, R. Y.; Liang, G. X.; Sham, T. K.; Sun, X. L. $LiFePO_4$-Graphene as a Superior Cathode Material for Rechargeable Lithium Batteries: Impact of Stacked Graphene and Unfolded Graphene. *Energy Environ. Sci.* **2013**, *6*, 1521−1528.
(9) Gao, Y.; Ma, D.; Hu, G.; Zhai, P.; Bao, X.; Zhu, B.; Zhang, B.; Su, D. S. Layered-Carbon-Stabilized Iron Oxide Nanostructures as Oxidation Catalysts. *Angew. Chem., Int. Ed.* **2011**, *50*, 10236−10240.
(10) Zhou, J. G.; Wang, J.; Zuin, L.; Regier, T.; Hu, Y. F.; Wang, H. L.; Liang, Y. Y.; Maley, J.; Sammynaiken, R.; Dai, H. J. Spectroscopic Understanding of Ultra-High Rate Performance for $LiMn_{0.75}Fe_{0.25}PO_4$

DOI: 10.1021/am5073996
ACS Appl. Mater. Interfaces 2015, 7, 7863−7868

Nanorods-Graphene Hybrid in Lithium Ion Battery. *Phys. Chem. Chem. Phys.* **2012**, *14*, 9578−9581.
(11) Sun, S.; Zhang, G.; Gauquelin, N.; Chen, N.; Zhou, J.; Yang, S.; Chen, W.; Meng, X.; Geng, D.; Banis, M. N.; et al. Single-Atom Catalysis Using Pt/Graphene Achieved through Atomic Layer Deposition. *Sci. Rep.* **2013**, *3*, 1775−1783.
(12) Wang, J.; Zhou, J. G.; Hu, Y. F.; Regier, T. Chemical Interaction and Imaging of Single Co_3O_4/Graphene Sheets Studied by Scanning Transmission X-ray Microscopy and X-ray Absorption Spectroscopy. *Energy Environ. Sci.* **2013**, *6*, 926−934.
(13) Guo, J. Synchrotron Radiation, Soft X-ray Spectroscopy and Nanomaterials. *Int. J. Nanotechnol.* **2004**, *1*, 193−225.
(14) Skytt, P.; Glans, P.; Mancini, D. C.; Guo, J. H.; Wassdahl, N.; Nordgren, J.; Ma, Y. Angle-Resolved Soft-X-ray Fluorescence and Absorption Study of Graphite. *Phys. Rev. B* **1994**, *50*, 10457−10461.
(15) Zhou, J.; Wang, J.; Liu, H.; Banis, M. N.; Sun, X.; Sham, T.-K. Imaging Nitrogen in Individual Carbon Nanotubes. *J. Phys. Chem. Lett.* **2010**, *1*, 1709−1713.
(16) Felten, A.; Bittencourt, C.; Pireaux, J.-J.; Reichelt, M.; Mayer, J.; Hernandez-Cruz, D.; Hitchcock, A. P. Individual Multiwall Carbon Nanotubes Spectroscopy by Scanning Transmission X-ray Microscopy. *Nano Lett.* **2007**, *7*, 2435−2440.
(17) Zhong, J.; Xie, T.; Deng, J.; Sun, X. H.; Pan, X. L.; Bao, X.; Wu, Z. Y. Direct Observation and Spectroscopy of Nanoscaled Carboxylated Carbonaceous Fragments Coated on Carbon Nanotubes. *Chem. Commun.* **2011**, *47*, 8373−8375.
(18) Jiménez-Villacorta, F.; Prieto, C.; Huttel, Y.; Telling, N. D.; van der Laan, G. X-ray Magnetic Circular Dichroism Study of the Blocking Process in Nanostructured Iron-Iron Oxide Core-Shell Systems. *Phys. Rev. B* **2011**, *84*, 172404−5.
(19) Nordgren, J.; Guo, J. Instrumentation for Soft X-ray Emission Spectroscopy. *J. Electron Spectrosc. Relat. Phenom.* **2000**, *110*−*111*, 1−13.
(20) Zhong, J.; Song, L.; Wu, Z. Y.; Xie, S.; Abbas, M.; Ibrahim, K.; Qian, H. X-ray Absorption near-Edge Structure and Photoelectron Spectroscopy of Single-Walled Carbon Nanotubes Modified by a HBr Solution. *Carbon* **2006**, *44*, 866−872.
(21) Kuznetsova, A.; Popova, I.; Yates, J. T.; Bronikowski, M. J.; Huffman, C. B.; Liu, J.; Smalley, R. E.; Hwu, H. H.; Chen, J. G. Oxygen-Containing Functional Groups on Single-Wall Carbon Nanotubes: NEXAFS and Vibrational Spectroscopic Studies. *J. Am. Chem. Soc.* **2001**, *123*, 10699−10704.
(22) Hemraj-Benny, T.; Banerjee, S.; Sambasivan, S.; Balasubramanian, M.; Fischer, D. A.; Eres, G.; Puretzky, A. A.; Geohegan, D. B.; Lowndes, D. H.; Han, W. Q.; et al. Near-Edge X-ray Absorption Fine Structure Spectroscopy as a Tool for Investigating Nanomaterials. *Small* **2006**, *2*, 26−35.
(23) Zhou, J. G.; Wang, J.; Fang, H.; Sham, T. K. Structural Variation and Water Adsorption of a SnO_2 Coated Carbon Nanotube: A Nanoscale Chemical Imaging Study. *J. Mater. Chem.* **2011**, *21*, 5944−5949.
(24) Yueh, C. L.; Jan, J. C.; Chiou, J. W.; Pong, W. F.; Tsai, M. H.; Chang, Y. K.; Chen, Y. Y.; Lee, Y. F.; Tseng, P. K.; Wei, S. L.; et al. Electronic Structure of the Fe-layer-catalyzed Carbon Nanotubes Studied by X-ray-Absorption Spectroscopy. *Appl. Phys. Lett.* **2001**, *79*, 3179−3181.
(25) Petit, T.; Pflüger, M.; Tolksdorf, D.; Xiao, J.; Aziz, E. F. Valence Holes Observed in Nanodiamonds Dispersed in Water. *Nanoscale* **2015**, *7*, 2987−2991.
(26) Carlisle, J. A.; Shirley, E. L.; Hudson, E. A.; Terminello, L. J.; Callcott, T. A.; Jia, J. J.; Ederer, D. L.; Perera, R. C. C.; Himpsel, F. J. Probing the Graphite Band Structure with Resonant Soft-X-ray Fluorescence. *Phys. Rev. Lett.* **1995**, *74*, 1234−1237.
(27) Lange, K. M.; Aziz, E. F. Electronic Structure of Ions and Molecules in Solution: A View from Modern Soft X-ray Spectroscopies. *Chem. Soc. Rev.* **2013**, *42*, 6840−6859.
(28) Park, J.; An, K.; Hwang, Y.; Park, J.-G.; Noh, H.-J.; Kim, J.-Y.; Park, J.-H.; Hwang, N.-M.; Hyeon, T. Ultra-Large-Scale Synthesis of Monodisperse Nanocrystals. *Nat. Mater.* **2004**, *3*, 891−895.
(29) Kronawitter, C. X.; Bakke, J. R.; Wheeler, D. A.; Wang, W.-C.; Chang, C.; Antoun, B. R.; Zhang, J. Z.; Guo, J.; Bent, S. F.; Mao, S. S.; et al. Electron Enrichment in 3d Transition Metal Oxide Heteronanostructures. *Nano Lett.* **2011**, *11*, 3855−3861.
(30) Perez, N.; Bartolome, F.; Garcia, L. M.; Bartolome, J.; Morales, M. P.; Serna, C. J.; Labarta, A.; Batlle, X. Nanostructural Origin of the Spin and Orbital Contribution to the Magnetic Moment in $Fe_{3-x}O_4$ Magnetite Nanoparticles. *Appl. Phys. Lett.* **2009**, *94*, 093108−10.
(31) Pearce, C. I.; Henderson, C. M. B.; Pattrick, R. A. D.; van der Laan, G.; Vaughan, D. J. Direct Determination of Cation Site Occupancies in Natural Ferrite Spinels by $L_{2,3}$ X-ray Absorption Spectroscopy and X-ray Magnetic Circular Dichroism. *Am. Mineral.* **2006**, *91*, 880−893.

DOI: 10.1021/am5073996
ACS Appl. Mater. Interfaces 2015, 7, 7863−7868